

## Molecular Insights into 14-Membered Macrolides Using the MM-PBSA Method

Wai Keat Yam<sup>†</sup> and Habibah A. Wahab<sup>\*,†,‡</sup>

Pharmaceutical Design and Simulation (PhDS) Laboratory, School of Pharmaceutical Sciences, Universiti Sains Malaysia, 11800 Minden, Pulau Pinang, Malaysia, and Division for Advanced Drug Delivery, Malaysian Institute of Pharmaceuticals and Nutraceuticals, Malaysian Ministry of Science, Technology and Innovation, SAINS@USM 10, Persiaran Bukit Jambul, 11900 Bukit Jambul, Pulau Pinang, Malaysia

Received September 24, 2008

Erythromycin A and roxithromycin are clinically important macrolide antibiotics that selectively act on the bacterial 50S large ribosomal subunit to inhibit bacteria's protein elongation process by blocking the exit tunnel for the nascent peptide away from ribosome. The detailed molecular mechanism of macrolide binding is yet to be elucidated as it is currently known to the most general idea only. In this study, molecular dynamics (MD) simulation was employed to study their interaction at the molecular level, and the binding free energies for both systems were calculated using the molecular mechanics Poisson–Boltzmann surface area (MM-PBSA) method. The calculated binding free energies for both systems were slightly overestimated compared to the experimental values, but individual energy terms enabled better understanding in the binding for both systems. Decomposition of results into residue basis was able to show the contribution of each residue at the binding pocket toward the binding affinity of macrolides and hence identified several key interacting residues that were in agreement with previous experimental and computational data. Results also indicated the contributions from van der Waals are more important and significant than electrostatic contribution in the binding of macrolides to the binding pocket. The findings from this study are expected to contribute to the understanding of a detailed mechanism of action in a quantitative matter and thus assisting in the development of a safer macrolide antibiotic.

### INTRODUCTION

Erythromycin A (ERYA) and roxithromycin (ROX) are prominent macrolide antibiotics introduced years ago and are clinically effective in the treatment of diseases caused by a wide range of bacteria. ERYA is one of the most important and effective macrolide antibiotics that is still widely in use today to treat infections caused by common bacterial pathogens and some nontypical pathogens.<sup>1–3</sup> It belongs to the first generation of the 14-membered ring macrolide and is produced by *Saccaropolyspora erythraea*.<sup>4</sup> ROX, on the other hand, is a second generation, semisynthetic macrolide antibiotic derived from ERYA.<sup>5</sup> It has a broader antibacterial spectrum and has a longer half-life and better absorption<sup>1</sup> than ERYA. It was also shown that ROX has higher inhibitory activity against Gram negative bacteria.<sup>6</sup> Both macrolides shared a similar chemical structure with a common 14-membered lactone ring, a desosamine sugar branched from position 5 of the lactone ring and cladinose sugar branched from the C-3 position of the lactone ring (Figure 1). However, the major difference of both macrolides is that ROX has an etheroxime chain sprouting at the C-9 position of the lactone ring.

The two macrolides have a similar mechanism of action, i.e. they inhibit the bacterial protein synthesis by selectively binding to the 50S large ribosomal subunit. The crystal structure showed that both macrolides interact exclusively

with Domain V of the 23S rRNA, at the entrance of the peptide exit tunnel in the peptidyl transferase center,<sup>7</sup> while other experimental studies revealed that these macrolides also interact with the Helix 35 of Domain II.<sup>6,8–12</sup> Besides that, our previous MD studies also demonstrated a possible interaction with the Domain IV.<sup>13</sup> These macrolides showed high drug affinity and specificity to the ribosome with  $K_d$  in the nanomolar range as measured by equilibrium dialysis,<sup>14</sup> footprinting protection experiments,<sup>6,9,15</sup> and binding kinetics<sup>16,17</sup> studies. The actual inhibition mode of ERYA and ROX to the bioactivity of ribosome is so far understood to the most general idea only. Therefore, to enable a rational approach for antibiotic development, a comprehensive understanding and elucidation of the drug inhibition at the molecular level is desired.

Here we attempt to address these issues by employing molecular dynamics (MD) simulation, complemented with energetic analysis using the MM-PBSA (molecular mechanics Poisson–Boltzmann surface area) method<sup>18,19</sup> for the complexes of the 50S ribosomal subunit and macrolides in aqueous solution. MD simulations of a large ribosomal subunit complexed with ERYA and ROX systems were performed for 2.5 ns. Preliminary MD results on a large ribosomal subunit complexed with the ERYA system has been reported,<sup>13</sup> and a further energetic analysis on this system is reported here. The MM-PBSA method was used to calculate the binding free energies of both systems comprising ERYA and ROX with the binding pocket in the 50S ribosomal subunit. The estimated binding free energies are slightly overestimated compared to the experimental

\* Corresponding author phone: (604)653-2206, (604)653-4533; fax: (604)642-7504; e-mail: habibah@ippharm.gov.my, habibahw@usm.my.

<sup>†</sup> Universiti Sains Malaysia.

<sup>‡</sup> Malaysian Ministry of Science, Technology and Innovation.

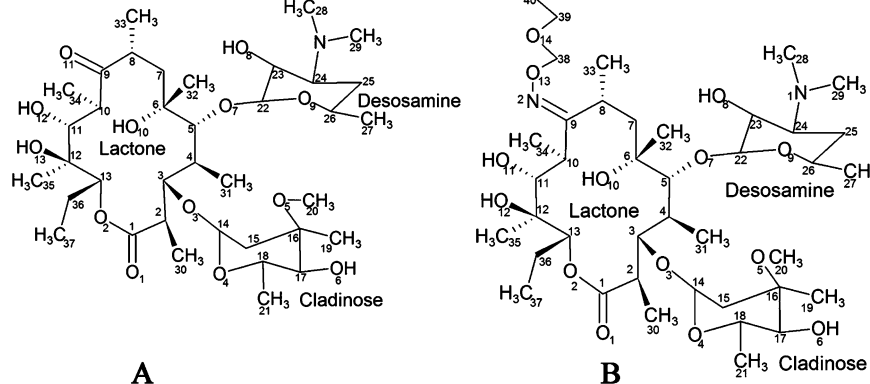


**Figure 1.** Chemical structures of ERYA (A) and ROX (B). Both macrolides have a 14-membered lactone ring, a desosamine sugar, and a cladinose sugar. A significant difference between both macrolides lies at position 9 of the lactone ring, where ROX has an etheroxime chain instead of a carbonyl group at the same position in ERYA. Drawing tool: ACD/ChemSketch Freeware (<http://www.acdlabs.com>).

**Table 1.** MD Systems Setup Details

systems	number of atoms in molecular structure	water molecules	neutralizing ions	total number of atoms
50S ribosomal subunit + ERYA	99,362	296,254	1400 K+ 1444 Na+	990,968
50S ribosomal subunit + ROX	99,378	296,220	1400 K+ 1445 Na+	990,883

determined values, and ERYA was found to exhibit more favorable interaction to the binding pocket when compared to ROX. The decomposition results of a residue-based nonbonded contribution toward the antibiotics showed insights into the interaction mechanism that was exerted by each interacting residue and thus quantified the molecular interactions that happen in the binding as observed in the MD simulations. Several residues have shown their importance when participating in making interaction with the binding pocket, where they were previously identified and mentioned in experimental and computational studies. Besides that, the results also indicated a more favorable and significant contribution from van der Waals than electrostatic in the binding of ERYA and ROX in both simulation systems. This study would be helpful and useful for the understanding of ribosomal subunit-macrolides interaction and hence facilitating research and development of rational antibiotics designing.

## METHODS

**Model Setup.** The initial three-dimensional structure of the 50S large ribosomal subunit complexed with ERYA (Protein Data Bank code: 1JZY<sup>7</sup>), including 23S rRNA, three chains of ribosomal proteins L4, L22, and L32, and two crystallographic magnesium ions, was used as a starting point. Residues that were missing from this X-ray crystal structure were reconstructed as described in ref 13, and all hydrogen atoms were added explicitly using the LEAP module of the AMBER 8 package.<sup>20</sup> The Amber 99 (RNA) all atom force field<sup>21</sup> was applied to describe the molecular mechanics for the ribosomal subunit, while the general amber force field (GAFF)<sup>22</sup> was used to describe the inhibitors. Geometries of the two inhibitors used, ERYA and ROX, were fully optimized, and their electrostatic potentials were obtained using single-point calculation, both at the B3LYP

level with the 6-31G(d,p) basis set using the GAUSSIAN 03<sup>23</sup> program. Subsequently, their partial charges were obtained by restrained electrostatic potential (RESP) using ANTECHAMBER.<sup>24</sup> Although the default charge scheme used along with GAFF is at the HF/6-31G(d) level,<sup>22</sup> we have utilized RESP charges at the B3LYP/6-31G(d,p) level to ensure higher accuracy and reliability for the two inhibitors that were involved in the study. Nevertheless, RESP charges for both inhibitors were also parametrized using the HF/6-31G(d) level of theory (in order to be consistent with the GAFF usage as highlighted in refs 22 and 25) and can be found in the Supporting Information. Potassium and sodium counterions were added to the most negative position of the complexes to ensure the systems' neutrality prior to solvation in the TIP3P<sup>26</sup> water box, yielding a large amount of atoms in the simulation systems as shown in Table 1.

**Minimization and MD Simulation.** Both minimizations and MD simulations were executed using the SANDER module of AMBER 8. A detailed procedure of minimization and MD simulation used in this study is described in ref 13. A total of 15,000 steps of minimizations were done using the Steepest Descent and Conjugate Gradient algorithms before proceeding to the heating and equilibration stages of MD simulations. Equilibration stages were done using the canonical ensemble before switching over to the NPT ensemble for production stage. The pressure of the systems were regulated at 1 bar with an isotropic position scaling using the Berendsen barostat,<sup>27</sup> and the temperature for both systems was maintained at 300 K using the Langevin thermostat with collision frequency of 1.0 ps<sup>-1</sup>.<sup>28</sup> The SHAKE algorithm was turned on to constrain bonds involving hydrogen to allow the integration of the force equation at 2 fs. Trajectories were saved at every 50 steps during the simulation for the later analysis, and the electrostatic interactions were properly corrected using Particle Mesh

Ewald (PME) with the nonbonded cutoff set to 8.0 Å. Minimizations and MD simulations for a large ribosomal subunit and the ERYA system were performed using a 16-CPU Linux cluster and SGI Altix 4700 for approximately 1106 h, while the system of the large ribosomal subunit and ROX was performed in SGI Altix 4700 for 956 h. Analysis of MD trajectories was focused on its production stage, while thermodynamics properties were monitored throughout the simulation. Energetic analysis was done from 500–2500 ps window, using MM-PBSA scripts by AMBER 8 (see below).

**MM-PBSA Calculation.** All energetic analyses were done using a single trajectory approach, where each large ribosomal subunit-inhibitor complex, large ribosomal subunit, and inhibitor snapshots were taken from the snapshot of the performed MD trajectory. According to the MM-PBSA method,<sup>18,19</sup> binding free energy ( $\Delta G_{\text{bind}}$ ) of each system could be conceptually summarized as follows

$$\Delta G_{\text{bind}} = G_{\text{com}} - G_{\text{rec}} - G_{\text{lig}} \quad (1)$$

$$\Delta G = \Delta E_{\text{MM}} + \Delta G_{\text{solv}} - T\Delta S \quad (2)$$

In which

$$\Delta E_{\text{MM}} = \Delta E_{\text{bond}} + \Delta E_{\text{angle}} + \Delta E_{\text{torsion}} + \Delta E_{\text{vdw}} + \Delta E_{\text{EEL}} \quad (3)$$

$$\Delta G_{\text{solv}} = \Delta G_{\text{PB}} + \Delta G_{\text{SA}} \quad (4)$$

$$\Delta G_{\text{SA}} = \gamma SA + b \quad (5)$$

where  $G_{\text{com}}$ ,  $G_{\text{rec}}$ , and  $G_{\text{lig}}$  are the free energy for the complex, receptor, and ligand (inhibitor), respectively. Each term is calculated by averaging the energy of molecular mechanics ( $\Delta E_{\text{MM}}$ ), the solvation free energy ( $\Delta G_{\text{solv}}$ ), and the vibrational entropy term ( $T\Delta S$ ) as in (2).  $\Delta E_{\text{MM}}$  (3) denotes the average molecular mechanics energy contributed by bonded ( $E_{\text{bond}}$ ,  $E_{\text{angle}}$ , and  $E_{\text{torsion}}$ ) and nonbonded ( $E_{\text{vdw}}$  and  $E_{\text{EEL}}$ ) terms, and the individual nonbonded contribution of the binding pocket to inhibitor was further decomposed on a residue basis using MM-PBSA.

$\Delta G_{\text{solv}}$  (4) is the solvation free energy given by  $\Delta G_{\text{PB}}$ , polar solvation free energy evaluated using the Poisson–Boltzmann equation, and  $\Delta G_{\text{SA}}$ , nonpolar contribution to solvation free energy from the surface area.<sup>29</sup> The electrostatic solvation free energy was calculated using DELPHI<sup>30,31</sup> software, with low dielectric medium for solute ( $\epsilon=1$ ) and high dielectric medium for solvent ( $\epsilon=80$ ). Atomic radii were taken from PARSE<sup>29</sup> with an additional value of 1.90 Å for phosphorus,<sup>32</sup> and in order to be consistent with molecular mechanics energy calculation, the partial charges on solute were taken from the Amber 99 (RNA) force field<sup>21</sup> and from our *ab initio* calculation (see above) for inhibitors. An 80% boxfill lattice with grid spacing 0.5 grid/Å was applied, and 10,000 linear iteration steps were required to obtain energy convergence. A nonpolar contribution to solvation free energy was determined from (5), where the surface area was calculated using molsurf from AMBER 8, and  $\gamma$  and  $b$  are 0.00542 kcal/mol Å<sup>2</sup> and 0.92 kcal/mol, respectively, for use with PARSE atomic radii.<sup>29</sup> The solvent probe radius was set to 1.4 Å. Residues within 25 Å from the mass center of ligand were used for PBSA calculation (this included the ligand with the exception of water molecules and ions), and a total

of 2000 snapshots were extracted from the last 2 ns of MD trajectory with an interval of 1 ps.

The solute entropy contribution ( $-T\Delta S$ ) was estimated by normal-mode analysis<sup>18</sup> using the NMODE module in AMBER 8.0. Each of the complex, receptor, and ligand systems were first minimized before switching over for normal-mode analysis, using a distance dependent dielectric constant of  $\epsilon = 4r$  ( $r$ =interatomic distance), in the absence of solvent to mimic solvent screening<sup>33</sup> until the convergence criteria of 0.0001 kcal/mol Å was achieved. Normal mode calculation was extremely time-consuming and computationally expensive for a large system; therefore, only residues within 10 Å from the mass center of inhibitor (excluding water molecules and ions) were used here. As discussed in refs 34 and 35 the differences of the calculated entropy value is quite small for different conformations, and normal-mode analysis calculation usually gave an inaccurate estimation for solute entropies, thus giving merely qualitative estimates of the solute entropy.<sup>36</sup> Therefore, our calculation was only based on the average entropy value obtained from 25 snapshots taken from the final 2000 ps MD trajectories with a time interval of 20 ps.

## RESULTS AND DISCUSSION

Over the 2.5 ns MD trajectories of the 50S ribosomal subunit with ERYA and ROX systems, the overall structure of both complexes appeared to be equilibrated after ~500 ps, as reflected by the potential energy (Figure 2A,B) and rms deviation plots (Figure 3A,B). The average rms deviation of the binding pocket (taken as 15 Å from the mass of inhibitors) relative to the starting structure was  $3.75 \pm 0.31$  Å and  $3.54 \pm 0.35$  Å for ERYA and ROX systems, respectively (Figure 3A). Both binding pockets deviated rapidly starting from 1700 ps but fluctuated at around 4.00 Å and 3.80 Å, respectively, for ERYA and ROX systems during 2000–2500 ps. On the other hand, the inhibitors were well maintained in the binding pocket where the average rms deviation for ERYA was found displaced about  $1.61 \pm 0.12$  Å from the initial structure and fluctuated in the range of 1.35–2.10 Å during the equilibration and production stages (Figure 3B). ROX has lower rms deviation values where it fluctuated in the range of 1.10–1.80 Å during the MD production stages and only deviated  $1.36 \pm 0.10$  Å on average (Figure 3B).

From the perspective of energetics, a summary of the MM-PBSA calculation, including the calculated binding free energies, the contribution of energy terms to  $\Delta G_{\text{bind}}$  from molecular mechanics, polar and nonpolar solvation energy, and solute entropy between inhibitors and its binding pocket, is presented in Table 2. The calculated binding free energies for binding pocket-ERYA was  $-40.13$  kcal/mol and was overestimated compared to the experimental value ranging from  $1.1 \times 10^{-8}$  M ( $\Delta G_{\text{exp}} = -10.92$  kcal/mol),<sup>17</sup>  $1.4 \times 10^{-8}$  M ( $\Delta G_{\text{exp}} = -10.78$  kcal/mol)<sup>6,9</sup> to  $3.6 \times 10^{-8}$  M ( $\Delta G_{\text{exp}} = -10.22$  kcal/mol),<sup>16</sup> as determined from footprinting protection experiments and slow binding kinetic studies, respectively. Similarly, in the 50S ribosomal subunit-ROX system, the calculated binding free energy for binding pocket-ROX was  $-28.30$  kcal/mol which was overestimated compared to the experimental value of  $-10.57$  kcal/mol ( $2.0 \times 10^{-8}$  M) obtained from slow binding kinetic studies.<sup>16</sup>

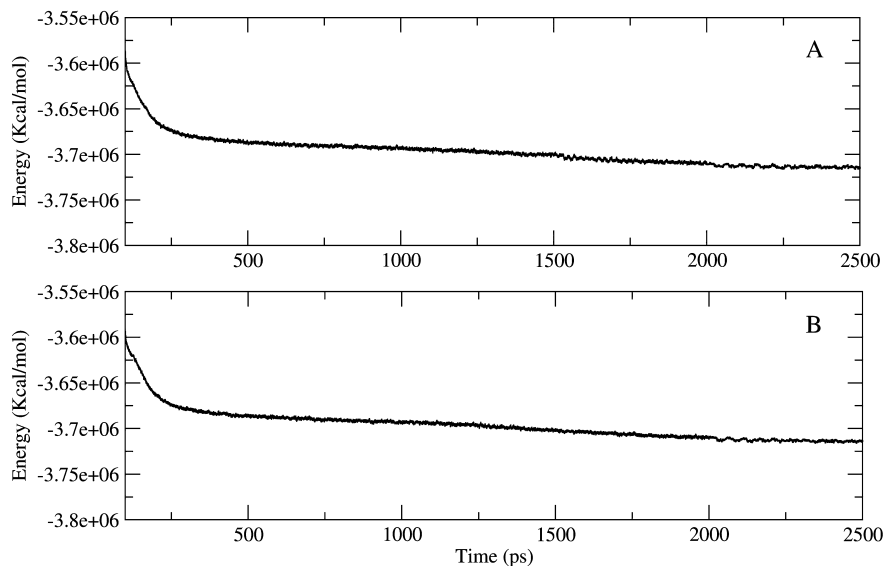


**Figure 2.** Potential energy plots for (A) the ERYA bound system and (B) the ROX bound system. The first 100 ps which are intended for heating are omitted. Plotting tool: Grace (<http://plasma-gate.weizmann.ac.il/Grace/>).

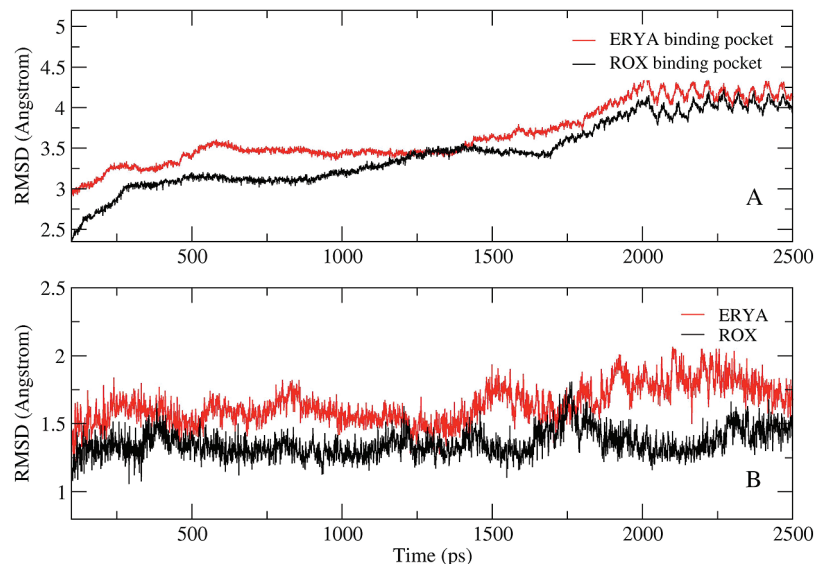


**Figure 3.** rms deviation plots for (A) backbone of the binding pocket for ERYA and ROX and (B) ERYA and ROX alone, with reference to the starting structure. The first 100 ps which were intended for heating and equilibration are omitted. Plotting tool: Grace (<http://plasma-gate.weizmann.ac.il/Grace/>).

The significant discrepancies in the calculated binding free energy and experimentally determined values might be due to the difference in conditions in both experiments, for example temperature (298 K and 310 K, respectively, for the kinetic experiment<sup>16,17</sup> and 310 K for the footprinting protection experiment<sup>6,9</sup>) versus 300 K for the present MD simulations. In addition to that, the difference in bacteria species for the ribosome structures used in both experiments and in this MD simulation might also be the contributory factors. The rate of inhibition for a drug varies for different species of bacteria used, since the ribosome structure used in experiments was that from *Escherichia coli*, the preferred source as pathogen representative, while the ribosome structure used in this MD simulations was from *Deinococcus radiodurans* (it is the only available crystal structure of ribosome complexed with ERYA and ROX to date). Nevertheless, *D. radiodurans* is an extremely robust Gram

positive mesophilic eubacterium, and it shares extensive similarity with the Gram negative eubacterium *Escherichia coli*.<sup>4,37</sup>

Table 2 showed major contributions to the binding free energy came from the van der Waals interaction ( $\Delta E_{VDW}$ ) with  $-78.62$  and  $-81.09$  kcal/mol from ERYA and ROX systems, respectively. There was variation in the electrostatic contributions with different systems;  $\Delta E_{EEL}$  for the ERYA pocket was favorable (negative  $\Delta E_{EEL}$ ), while the ROX pocket has a positive  $\Delta E_{EEL}$  contribution. This might be due to the difference at the macrolide structures, where ROX has an additional etheroxime chain replacing the OH group at position 9 of the lactone ring of ERYA. The etheroxime chain has three OH groups and has an additional amide group that could have increased the electrostatic term in the ROX binding pocket. Besides that, the electrostatic solvation energies for both systems were found to be unfavorable (positive  $\Delta G_{PB}$ ), while the nonpolar solvation free energies

**Table 2.** Binding Free Energy and Other Energy Terms to  $\Delta G_{\text{bind}}$  for Binding Pocket-ERYA and Binding Pocket-ROX

contribution	binding pocket-ERYA (kcal/mol)	binding pocket-ROX (kcal/mol)
$\Delta E_{\text{EEL}}$	-4.16	10.33
$\Delta E_{\text{vdw}}$	-78.62	-81.09
$\Delta E_{\text{MM}}$	-82.78	-70.76
$\Delta G_{\text{PB}}$	30.68	27.52
$\Delta G_{\text{SA}}$	-8.35	-9.75
$\Delta G_{\text{MM-PBSA}}$	-60.44	-52.99
$-T\Delta S$	20.31	24.69
$\Delta G_{\text{bind}}$	-40.13	-28.30
$\Delta G_{\text{bind}} (\text{exp})$	-10.92 to -10.22	-10.57

The corresponding experimental  $\Delta G_{\text{bind}} (\text{exp})$  values were obtained using a  $K_{\text{diss}}$  value from refs 6, 9, 16, and 17 with the following relationship:<sup>35,45</sup>  $\Delta G_{\text{bind}} (\text{exp}) = RT \ln K_{\text{diss}} = RT \ln (IC_{50} + 0.50C_{\text{enz}}) \approx RT \ln IC_{50}$ , where R is the ideal gas constant, T is temperature (300 K is used here), and  $C_{\text{enz}}$  is the concentration of enzyme.

$(\Delta G_{\text{SA}})$  for both systems are favorable indicating hydrophobic interaction as the main contribution in their bindings.

The calculated binding free energies obtained from both systems suggested ERYA was more favorable in binding as compared to ROX. This observation was found to be inconsistent with previous experimental studies, where ROX has been demonstrated to be more favorable and superior as an antimicrobial agent against a different range of Gram positive and Gram negative bacteria<sup>4,16,38,39</sup> as compared to ERYA. This inconsistency could be due to the insufficient MD sampling or artifacts from the MM-PBSA calculation. Nevertheless, based on the obtained values for  $\Delta G_{\text{SA}}$ , we were able to show ROX renders more hydrophobicity to the system compared to ERYA, as ROX (a derivative of parent compound, ERYA) was more hydrophobic than the parent compound.<sup>40</sup>

Several studies<sup>35,41–46</sup> have shown a good correlation with experimental results when adapting MM-PBSA in studying the binding free energy of inhibitors to receptor, and consequently in-depth information about the binding mode of inhibitors to the receptor could be acquired. Nevertheless, there were a number of issues associated with MM-PBSA that need careful consideration when one wants to employ this method, and one of them is to justify the necessity to evaluate snapshots of the complex, receptor, and ligand from a single trajectory or running separate trajectories for all three terms. The single trajectory method has the apparent advantage as only one trajectory of the complex is needed; however, assumptions have to be made as snapshots of receptor and ligand taken from the trajectory of complex are of equivalent free energy to those that would be taken from separate trajectories.<sup>18,47</sup> As demonstrated by Kuhn and co-workers,<sup>48</sup> the use of MM-PBSA on a single, relaxed complex structure is adequate to provide a good binding affinity ranking and give a fair correlation with an experimental value. In our study, we opted for a single trajectory approach as well because there were no significant conformational changes upon binding in both systems when compared to the conformation of unbound ribosome as observed in our MD simulations (as shown in the Supporting Information).

Another issue when dealing with MM-PBSA is the approximation of the solute entropy. The calculation of solute

**Table 3.** Residue Based Decomposition of the Interaction Energies (kcal/mol) for van der Waals ( $\Delta E_{\text{vdw}}$ ) and Electrostatic ( $\Delta E_{\text{EEL}}$ ) between ERYA and Binding Pocket

residue number	$\Delta E_{\text{vdw}}$	$\Delta E_{\text{EEL}}$
C759	-0.67	-0.79
C765	-0.50	-0.40
C1773	-0.98	-1.99
A2040	-0.17	-0.25
A2041	-0.46	-0.20
A2042	-4.72	-0.62
G2044	-2.24	-0.84
A2045	-3.00	-0.65
C2046	-2.38	0.16
A2418	-1.68	0.18
A2430	-0.35	0.09
A2482	-1.44	-0.43
G2484	-1.74	-0.51
G2562	-0.76	-0.92
U2564	-1.33	-0.08
C2565	-3.29	0.45
U2588	-1.32	0.21
C2589	-3.69	0.74
U2590	-3.97	-0.42
$\Delta E_{\text{subtot}}$	-34.69	-6.27

entropy term using normal-mode analysis is normally time-consuming, computationally expensive, and difficult to converge in the calculation, and most of the time it can be omitted<sup>18,35,41</sup> when calculating binding free energy. Our MD simulation showed that this term cannot be omitted if one wants to have a clearer picture on the energy terms. As shown in Table 2, the initial  $\Delta G_{\text{bind}}$  values (excluding solute entropy) for binding pocket-ERYA and binding pocket-ROX were -60.44 and -52.99 kcal/mol, respectively and one can see that these values were far from the final  $\Delta G_{\text{bind}}$  and experimentally determined values. The solute entropy contribution calculated from normal-mode analysis was 20.31 kcal/mol for the binding pocket-ERYA system and 24.69 kcal/mol for the binding pocket-ROX system, and it has significantly reduced the estimated binding free energy to -40.13 and -28.30 kcal/mol in both systems. Since the deviation of each computed solute entropy value among different conformations in the sampling time interval is not very significant, a small number of snapshots are sufficient to give ample sampling for solute entropy values.<sup>44</sup> The solute entropy term calculated in this study was adapted from the method used in ref 35, by using a smaller area (10 Å from the mass center of the inhibitor) and with a bigger time interval (20 ps) extracted from the MD trajectory. This method has significantly expedited the normal-mode analysis calculation process and gave a qualitative estimation of solute entropy needed to calculate the binding free energy.

The overall binding free energies of ERYA and ROX on the binding pocket were also decomposed into electrostatic and van der Waals contribution using the same method (Tables 3 and 4). The residue based decomposition into electrostatic and van der Waals contribution is a good way to further quantify contribution of individual residues to the overall binding. It was previously proven that free energies could be unambiguously decomposed into contributions of different atom groups or their type of interactions using the more rigorous Free Energy Perturbation (FEP) approach as highlighted in refs 49 and 50. In this study, however, the use of the rigorous FEP approach on the current ribosomal-macrolide complexed systems are computationally expensive and are not possible with the current

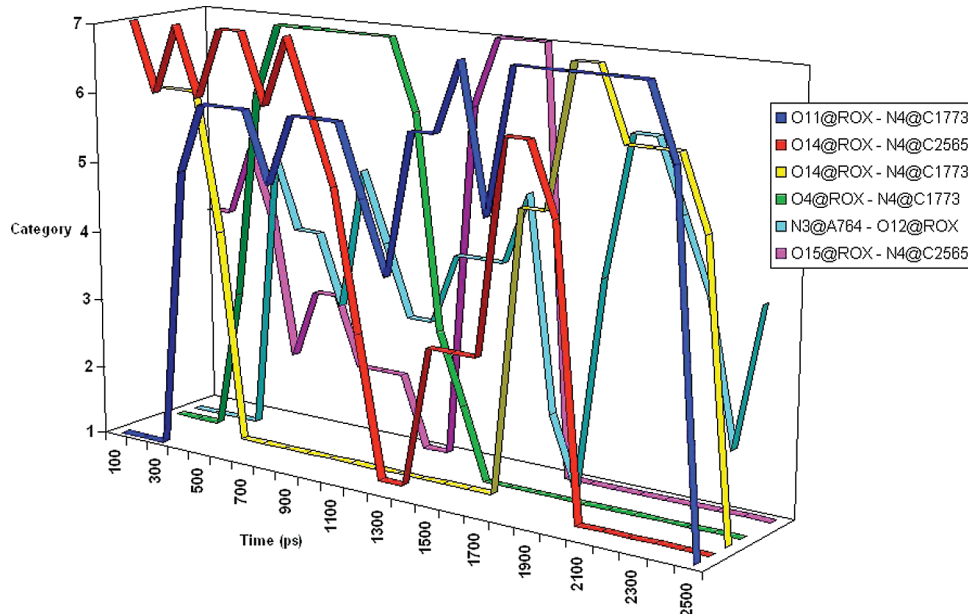


**Figure 4.** Time evolution of hydrogen bond occupancy for hydrogen bonds with occupancy >20% in the ROX system. Category 1 indicated percentage occupancy of hydrogen bonds for 0–5%, category 2 for 5–20%, category 3 for 20–40%, category 4 for 40–60%, category 5 for 60–80%, category 6 for 80–95%, and category 7 for 95–100%.

available computational facilities. Due to the employment of a less expensive way, the MM-PBSA has managed to provide this valuable piece of information at a reasonable basis. Nevertheless, it should be noted that a rigorous decomposition method should be employed to get more accurate insight into the contribution of residues.

Based on the decomposition results on the binding pocket-ERYA system (Table 3), the residue that exerted the strongest attraction toward ERYA was A2042 (A2059EC) (nucleotides are numbered according to *D. radiodurans*, unless stated in parentheses with *E. coli* (EC) numbers, here and throughout the entire manuscript) with  $-4.72$  kcal/mol from the van der Waals term and  $-0.62$  kcal/mol from the electrostatic term. This nucleotide was previously demonstrated to be important, as it formed a hydrogen bond with macrolides<sup>7,51</sup> and was strongly protected by ERYA from chemical modification.<sup>8,9,15,52,53</sup> Previous drug resistant mutation studies on adenine of 2059EC to cytosine<sup>11,54,55</sup> and guanine<sup>11,55</sup> also demonstrated the importance of this residue in drug binding. Visual inspection (Figure 4A) showed that the purine ring of A2042 was located directly on top of the desosamine sugar of ERYA, thus forming a strong and favorable stacking interaction between the purine base of A2042 and ERYA.

Similarly for U2590 (C2611EC), the pyrimidine base of U2590 was located almost parallel to the 14-membered lactone ring of ERYA, forming a face to face  $\pi-\pi$  interaction, with van der Waals and electrostatic energy terms of  $\Delta E_{vdw} = -3.97$  kcal/mol and  $\Delta E_{EEL} = -0.42$  kcal/mol, respectively. The importance of this residue was previously shown by its ability to form a hydrogen bond with macrolides<sup>7</sup> and in several point mutation studies where cytosine 2611EC was mutated to either guanine, uracil, or adenine.<sup>2,8,11,56</sup> C2565 (U2586EC) and C2589 (C2610EC) were also important in keeping both ERYA and ROX in the binding pocket (Tables 3 and 4). The position for the cytosine base of 2565 was directly on top of the macrolides' cladinose sugar and yielded a considerable favorable dispersive term ( $\Delta E_{vdw} = -3.29$  kcal/mol for binding pocket-ERYA,  $\Delta E_{vdw} = -2.16$  kcal/mol for binding pocket-ROX).

C2589 contributed a significant favorable van der Waals term to both ERYA and ROX of  $-3.69$  and  $-2.42$  kcal/mol, respectively. This might be due to the pyrimidine base of C2589 that was oriented side by side to the cladinose sugar, forming a stabilizing aromatic interaction between them. It is different in the case of the electrostatic term, where it yielded a nonfavorable term to ERYA with  $0.74$  kcal/mol but contributed a favorable and significant term of  $-1.54$  kcal/mol to ROX.

One of the most important and significant steric roles was played by C1773 (U1782EC) from the Domain IV of the 50S ribosomal subunit. Domain IV was discussed before to have exerted direct interaction with the binding of ERYA on the 50S ribosomal subunit.<sup>13</sup> Besides that, the quinolallyl group of ketolide ABT-773 was shown to have hydrophobic interaction to C1773 in the crystal structure of the large ribosomal subunit from *Deinococcus radiodurans* complexed with azithromycin and ketolide ABT-773.<sup>57</sup> In our study, C1773 has the most favorable Coulombic contribution to ERYA with the value of  $-1.99$  kcal/mol, and it has also a favorable van der Waals energy term of  $-0.98$  kcal/mol. In the ROX system, it has the most favorable dispersive term with  $-5.13$  kcal/mol and an electrostatic contribution of  $-0.89$  kcal/mol. These findings might be very significant in the overall binding of both ERYA and ROX with the binding pocket. It is possible that this was due to its contribution in forming five different hydrogen bonds from its O2, N3, and N4 of the cytosine base with O12 and O13 of the lactone ring for ERYA<sup>13</sup> and forming another three different hydrogen bonds through its N4 of the cytosine base to O11 of the lactone ring, O4 of the cladinose sugar, and O14 of the etheroxime chain from ROX (Table 5).

The hydrogen bonds accounted for ROX binding from C1773 were classified as persistent and medium hydrogen bonds according to the hydrogen bond classification.<sup>58</sup> The hydrogen bond between hydrogen N4 of the cytosine base and O11 at the lactone ring of ROX has 66.76% occupancy during the 2.5 ns simulation with the average distance and angle of  $3.09 \text{ \AA}$  and  $151.80^\circ$ , respectively. This bond was observed as a weak

**Table 4.** Residue Based Decomposition of the Interaction Energies (kcal/mol) for van der Waals ( $\Delta E_{vdw}$ ) and Electrostatic ( $\Delta E_{EEL}$ ) between ROX and Binding Pocket

residue number	$\Delta E_{vdw}$	$\Delta E_{EEL}$
G758	-0.1	-0.36
G761	-0.51	-0.56
A764	-2.30	-2.06
C765	-0.42	0.02
C803	-2.34	-0.24
C804	-1.28	0.43
G805	-0.41	-0.05
C1772	-0.61	0.39
C1773	-5.13	-0.89
A2040	-0.19	-0.15
A2041	-1.71	-0.20
A2042	-2.62	0.55
G2044	-1.24	0.32
A2045	-1.69	0.78
A2482	-1.30	-0.31
G2484	-1.33	-0.08
U2564	-1.35	0.13
C2565	-2.16	1.09
A2566	-0.77	0.81
G2587	-0.57	-0.40
U2588	-1.42	0.11
C2589	-2.42	-1.54
U2590	-0.95	-0.60
$\Delta E_{\text{subtot}}$	-32.82	-2.81

hydrogen bond at the beginning of the simulation but became stronger after 500 ps, until the end of the simulation (Figure 4). The hydrogen bond between N4 of the cytosine base and O14 of the etheroxime chain of ROX was observed in the beginning of the simulation with high occupancies. However this bond diminished after 400 ps but reoccurred at 1700 ps and maintained strong until 2300 ps. This bond has average occupancies of 34.52%, with average distances of 3.05 Å and 146.82°. Another hydrogen bond (N4@C1773 to O4@ROX) has an occupancy of 30.92% and an average length and angle of 3.11 Å and 146.80°, respectively. It was not formed in the beginning of the simulation but was persistent and had a strong presence during 500–1100 ps. However, this hydrogen bond started to decay after that period of time and finally deformed by 1500 ps. Besides explicit analysis of the hydrogen bond in both simulation systems, a detailed assessment was also done on the position of C1773 in the binding pocket. It was found that C1773 was at a proximal distance to A764 and C765 (from Domain II) (Figure 4A,B), and the exposure of this residue to ERYA and ROX became obvious in the production stage of MD simulations making it in a favorable position to make hydrogen bonds and aromatic interaction with the macrolides.

The decomposition results also agreed on the contribution of A2041 (A2058EC) and G2484 (G2505EC), as highlighted in refs 6–9 and 15, toward the binding of ERYA and ROX. Our simulation showed both A2041 and G2484 were involved mainly in a hydrophobic contribution toward ERYA<sup>13</sup> and were favorable to the binding of ERYA to the binding pocket with its van der Waals and electrostatic contribution ( $\Delta E_{vdw} = -0.46$  kcal/mol and  $\Delta E_{EEL} = -0.20$  kcal/mol for A2041;  $\Delta E_{vdw} = -1.74$  kcal/mol and  $\Delta E_{EEL} = -0.51$  kcal/mol for G2484). However, these residues exerted stronger van der Waals interaction with ROX than with ERYA with  $\Delta E_{vdw} = -1.71$  and  $-1.33$  kcal/mol, respectively.

Our studies also showed direct interaction of ERYA and ROX to Domain II of the 23S rRNA. Energetic decomposition results showed significant contributions from both van

der Waals and electrostatic energy terms for C759 and C765 from the ribosomal subunit-ERYA system and A764 and C803 (from the ribosomal subunit-ROX system) of Domain II. C759 has a total nonbonded contribution of  $-1.46$  kcal/mol ( $\Delta E_{vdw} = -0.67$  kcal/mol,  $\Delta E_{EEL} = -0.79$  kcal/mol) to ERYA, while contribution from van der Waals and electrostatics between C765 and ERYA were  $-0.50$  and  $-0.40$  kcal/mol, respectively. Their contributions toward ERYA in terms of hydrogen bond and hydrophobic interactions have previously been reported.<sup>13</sup> A764 has a significant total nonbonded contribution of  $-4.36$  kcal/mol toward ROX. Besides contributing  $\pi-\pi$  interaction, this residue was also involved in forming a medium hydrogen bond between its N3 at the purine base and hydrogen of O12 from the lactone ring of ROX. It has a percentage occupancy of 31.80%, with 3.25 Å and 149.62° for average distance and angle, respectively (Table 5). However, this hydrogen bond only formed after 600 ps and maintained moderately until 1700 ps. The bond was deformed at 1800 ps but reformed at 1900 ps and stayed until the end of the simulation (Figure 4). C803 has a favorable van der Waals contribution of  $-2.34$  kcal/mol, and this might due to the edge-on stacking that formed between the ribose sugar of this cytosine to the lactone ring of ROX (Figure 5B). These observations strongly agree with the protection effect found on hairpin 35 of Domain II in footprinting experiments<sup>6,8,9</sup> and therefore supported the speculation that the Domain II has direct and significant interactions with the macrolides.

## CONCLUSION

Results obtained from the application of the molecular mechanics Poisson–Boltzmann surface area (MM-PBSA) method on the evaluation of the binding free energy of 50S ribosomal subunit-ERYA and 50S ribosomal subunit-ROX systems enabled us to quantify their interactions at the molecular level. The calculated binding free energies of both systems were found to be overestimated as compared to the experimentally determined value. Nevertheless, itemized data of the contributed energy terms enabled us to understand better on the energy contributions to binding for both systems. Both systems have a high contribution from the van der Waals term in the binding of macrolides to the binding pocket, and the additional etheroxime chain at ROX is believed to render and disfavor the electrostatic contribution in the binding pocket.

From our decomposition results as calculated using MM-PBSA, we found that van der Waals interactions, when compared to electrostatic interactions, made very favorable binding between both drugs and nucleotides at the binding pocket. The total van der Waals contribution (summation of residue-based decomposition results in the binding pocket) exerted to ERYA from the binding pocket was  $-34.69$  kcal/mol, which is approximately 6 times stronger than the contribution from the Coulombic term ( $-6.27$  kcal/mol). Similar results were also observed in the binding pocket-ROX system, where the total van der Waals terms were clearly more favorable than the electrostatic terms. These quantitative results thereby supported the speculation that other nonbonded interactions, besides hydrogen bonds, exist in keeping ERYA and ROX in their binding pocket. Furthermore, decomposition results using residue basis also enabled us to understand explicitly the

**Table 5.** Hydrogen Bond Formed between ROX and Its Binding Pocket during the 2.5 ns MD Simulation<sup>a</sup>

hydrogen bond acceptor	hydrogen bond donor	percentage occupancy (%)	average distance (Å)	average angle (°)
O11@ROX	H4…N4@C1773	66.76	3.09	151.80
O14@ROX	H41…N4@C2565	41.20	3.07	150.47
O14@ROX	H41…N4@C1773	34.52	3.05	146.82
N3@A764	H36…O12@ROX	31.80	3.25	149.62
O4@ROX	H41…N4@C1773	30.92	3.11	146.80
O15@ROX	H41…N4@C2565	25.52	3.13	143.49

<sup>a</sup> H-bond distance and angle cut-off used in this analysis 3.5 Å and 120°, respectively.

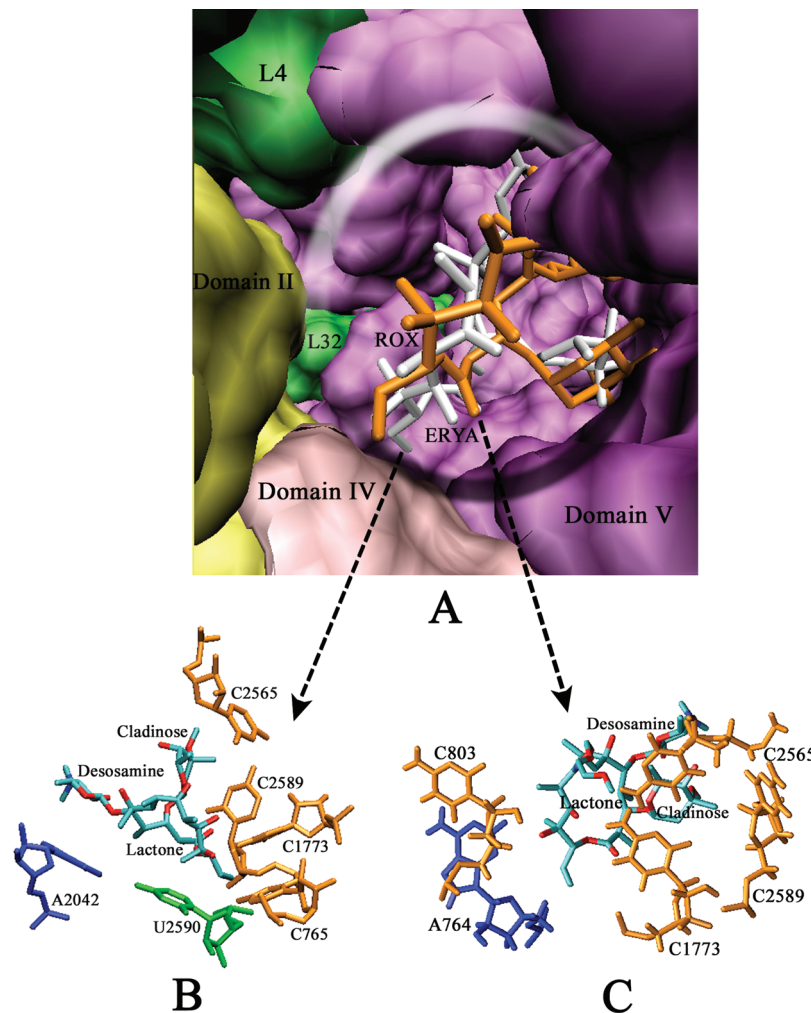


**Figure 5.** (A) Close-up surf representation of residues located 10 Å from the mass center of ERYA (white) and ROX (orange). Purple surface represents Domain V, pink for Domain IV, yellow for Domain II, and green for ribosomal proteins L4 and L32. Average MD structures of licorice representation of ERYA (B), ROX (C), and some interacting nucleotide residues in the binding pocket are shown here. Nucleotide in blue indicated adenine, orange indicated cytosine, and green for uracil. All hydrogen atoms and other residues are removed for clarity. Figures were illustrated using VMD.<sup>59</sup>

contribution of each residue to the binding of ERYA and ROX and thus correlate them with relevant physicochemical interactions as observed in the MD trajectories. This analysis is important to quantify their interaction and therefore provide qualitative results concerning macrolide interaction on the 50S ribosomal subunit.

#### ACKNOWLEDGMENT

This work was supported by the Ministry of Science, Technology and Innovation (MOSTI) grant (304/PFARMASI/640038/K105). We thank MIMOS Berhad for generously providing us with computational time.

**Supporting Information Available:** Comparison of rms deviation of unbound and bound macrolide binding pocket at the 50S ribosomal subunit and parametrization of both inhibitors at HF/6-31G(d) along with applied atom names, atom types, and RESP partial atomic charges. This material is available free of charge via the Internet at <http://pubs.acs.org>.

#### REFERENCES AND NOTES

- (1) Pal, S. A journey across the sequential development of macrolides and ketolides related to erythromycin. *Tetrahedron* **2006**, *62* (14), 3171–3200.
- (2) Nilius, A. M.; Ma, Z. Ketolides: the future of the macrolides. *Curr. Opin. Pharmacol.* **2002**, *2* (5), 493–500.

- (3) Gasc, J. C.; d'Ambrieres, S. G.; Lutz, A.; Chantot, J. F. New ether oxime derivatives of erythromycin A. A structure-activity relationship study. *J. Antibiot. (Tokyo)* **1991**, *44* (3), 313–330.
- (4) Auerbach, T.; Bashan, A.; Harms, J.; Schluenzen, F.; Zarivach, R.; Bartels, H.; Agmon, I.; Kessler, M.; Pioletti, M.; Franceschi, F.; Yonath, A. Antibiotics targeting ribosomes: crystallographic studies. *Curr. Drug Targets Infect. Disord.* **2002**, *2* (2), 169–186.
- (5) Kanfer, I.; Skinner, M. F.; Walker, R. B. Analysis of macrolide antibiotics. *J. Chromatogr.* **A** **1998**, *812* (1–2), 255–286.
- (6) Douthwaite, S.; Hansen, L. H.; Mauvais, P. Macrolide-ketolide inhibition of MLS-resistant ribosomes is improved by alternative drug interaction with domain II of 23S rRNA. *Mol. Microbiol.* **2000**, *36* (1), 183–193.
- (7) Schluenzen, F.; Zarivach, R.; Harms, J.; Bashan, A.; Tocilj, A.; Albrecht, R.; Yonath, A.; Franceschi, F. Structural basis for the interaction of antibiotics with the peptidyl transferase centre in eubacteria. *Nature* **2001**, *413* (6858), 814–821.
- (8) Xiong, L.; Shah, S.; Mauvais, P.; Mankin, A. S. A ketolide resistance mutation in domain II of 23S rRNA reveals the proximity of hairpin 35 to the peptidyl transferase centre. *Mol. Microbiol.* **1999**, *31* (2), 633–639.
- (9) Hansen, L. H.; Mauvais, P.; Douthwaite, S. The macrolide-ketolide antibiotic binding site is formed by structures in domains II and V of 23S ribosomal RNA. *Mol. Microbiol.* **1999**, *31* (2), 623–631.
- (10) Weisblum, B. Insights into erythromycin action from studies of its activity as inducer of resistance. *Antimicrob. Agents Chemother.* **1995**, *39* (4), 797–805.
- (11) Vester, B.; Douthwaite, S. Macrolide resistance conferred by base substitutions in 23S rRNA. *Antimicrob. Agents Chemother.* **2001**, *45* (1), 1–12.
- (12) Xiong, L.; Korkhin, Y.; Mankin, A. S. Binding site of the bridged macrolides in the Escherichia coli ribosome. *Antimicrob. Agents Chemother.* **2005**, *49* (1), 281–288.
- (13) Wahab, H. A.; Yam, W. K.; Samian, M. R.; Najimudin, N. Refinement of a Low-resolution Crystal Structure to Better Understand Erythromycin Interactions on Large Ribosomal Subunit. *J. Biomol. Struct. Dyn.* **2008**, *26* (1), 131–146.
- (14) Pestka, S.; Lemahieu, R. A. Effect of erythromycin analogues on binding of [<sup>14</sup>C]erythromycin to Escherichia coli ribosomes. *Antimicrob. Agents Chemother.* **1974**, *6* (4), 479–488.
- (15) Douthwaite, S.; Aagaard, C. Erythromycin binding is reduced in ribosomes with conformational alterations in the 23 S rRNA peptidyl transferase loop. *J. Mol. Biol.* **1993**, *232* (3), 725–731.
- (16) Dinos, G. P.; Connell, S. R.; Nierhaus, K. H.; Kalpaxis, D. L. Erythromycin, roxithromycin, and clarithromycin: use of slow-binding kinetics to compare their in vitro interaction with a bacterial ribosomal complex active in peptide bond formation. *Mol. Pharmacol.* **2003**, *63* (3), 617–623.
- (17) Lovmar, M.; Tenson, T.; Ehrenberg, M. Kinetics of macrolide action: the josamycin and erythromycin cases. *J. Biol. Chem.* **2004**, *279* (51), 53506–53515.
- (18) Kollman, P. A.; Massova, I.; Reyes, C.; Kuhn, B.; Huo, S.; Chong, L.; Lee, M.; Lee, T.; Duan, Y.; Wang, W.; Donini, O.; Cieplak, P.; Srinivasan, J.; Case, D. A.; Cheatham, T. E. 3rd. Calculating structures and free energies of complex molecules: combining molecular mechanics and continuum models. *Acc. Chem. Res.* **2000**, *33* (12), 889–897.
- (19) Kuhn, B.; Donini, O.; Huo, S.; Wang, J. M.; Kollman, P. A. MM-PBSA applied to computer-assisted ligand design. In *Free energy calculations in rational drug design*; Rami Reddy, M.; Erion, M. D., Eds.; Kluwer Academic/Plenum Publishers: New York, 2001; pp 243–251.
- (20) Case, D. A.; Darden, T. A.; Cheatham, T. E. I.; Simmerling, C. L.; Wang, J.; Duke, R. E.; Luo, R.; Merz, K. M.; Wang, B.; Pearlman, D. A.; Crowley, M.; Brozell, S.; Tsui, V.; Gohlke, H.; Mongan, J.; Hornak, V.; Cui, G.; Beroza, P.; Schafmeister, C.; Caldwell, J. W.; Ross, W. S.; Kollman, P. A. *AMBER 8, 8.0 edn*; University of California: San Francisco, CA, 2004.
- (21) Cornell, W. D.; Cieplak, P.; Bayly, C. I.; Gould, I. R.; Merz, K. M. J.; Ferguson, D. M.; Spellmeyer, D. C.; Fox, T.; W., C. J.; Kollman, P. A. A second generation force field for the simulation of proteins, nucleic acids and organic molecules. *J. Am. Chem. Soc.* **1995**, *117*, 5179–5197.
- (22) Wang, J.; Wolf, R. M.; Caldwell, J. W.; Kollman, P. A.; Case, D. A. Development and testing of a general AMBER force field. *J. Comput. Chem.* **2004**, *25* (9), 1157–1174.
- (23) Frisch, M. J.; Trucks, G. W.; Schlegel, H. B.; Scuseria, G. E.; Robb, M. A.; Cheeseman, J. R.; Montgomery, J. A. J.; Vreven, T.; Kudin, K. N.; Burant, J. C.; Millam, J. M.; Liyengar, S. S.; Tomasi, J.; Barone, V.; Mennucci, B.; Cossi, M.; Scalmani, G.; Rega, N.; Petersson, G. A.; Nakatsuji, H.; Hada, M.; Ehara, M.; Toyota, K.; Fukuda, R.; Hasegawa, J.; Ishida, M.; Nakajima, T.; Honda, Y.; Kitao, O.; Nakai, H.; Klene, M.; Li, X.; Knox, J. E.; Hratchian, H. P.; Cross, J. B.; Bakken, V.; Adamo, C.; Jaramillo, J.; Gomperts, R.; Stratmann, R. E.; Yazyev, O.; Austin, A. J.; Cammi, R.; Pomelli, C.; Ochterski, J. W.; Ayala, P. Y.; Morokuma, K.; Voth, G. A.; Salvador, P.; Dannenberg, J. J.; Zakrzewski, V. G.; Dapprich, S.; Daniels, A. D.; Scalmani, G.; Farkas, O.; Malick, D. K.; Rabuck, A. D.; Raghavachari, K.; Foresman, J. B.; Ortiz, J. V.; Cui, Q.; Baboul, A. G.; Clifford, S.; Cioslowski, J.; Stefanov, B. B.; Liu, G.; Liashenko, A.; Piskorz, P.; Komaromi, I.; Martin, R. L.; Fox, D. J.; Keith, T.; Al-Laham, M. A.; Peng, C. Y.; Nanayakkara, A.; Challacombe, M.; Gill, P. M. W.; Johnson, B.; Chen, W.; Wong, M. W.; Gonzalez, C.; Pople, J. A. *Gaussian 03, Revision C.02*; Gaussian, Inc.: Wallingford, CT, 2004.
- (24) Wang, J. M.; Wang, W.; Kollman, P. A. Antechamber: An accessory software package for molecular mechanical calculations. *Abstr. Pap. Am. Chem. Soc.* **2001**, *222*, U403–U403.
- (25) Bren, U.; Hodosek, M.; Koller, J. Development and validation of empirical force field parameters for netropsin. *J. Chem. Inf. Model.* **2005**, *45* (6), 1546–1552.
- (26) Jorgensen, W. L.; Chandrasekhar, J.; Madura, J. D.; Impey, R. W.; Klein, M. L. Comparison of simple potential functions for simulating liquid water. *J. Chem. Phys.* **1983**, *79*, 926–935.
- (27) Berendsen, H. J. C.; Postma, J. P. M.; Van Gunsteren, W. F.; Dinola, A.; Haak, J. Molecular-dynamics with coupling to an external bath. *J. Chem. Phys.* **1984**, *81*, 3684–3690.
- (28) Pastor, R. W.; Brooks, B. R.; A., S. An analysis of the accuracy of Langevin and molecular dynamics algorithms. *Mol. Phys.* **1988**, *65*, 1409–1419.
- (29) Sitkoff, D.; Sharp, K. A.; Honig, B. Accurate Calculation of Hydration Free-Energies Using Macroscopic Solvent Models. *J. Phys. Chem.* **1994**, *98* (7), 1978–1988.
- (30) Rocchia, W.; Sridharan, S.; Nicholls, A.; Alexov, E.; Chiabrera, A.; Honig, B. Rapid grid-based construction of the molecular surface and the use of induced surface charge to calculate reaction field energies: Applications to the molecular systems and geometric objects. *J. Comput. Chem.* **2002**, *23* (1), 128–137.
- (31) Honig, B.; Sharp, K.; Yang, A. S. Macroscopic Models of Aqueous-Solutions - Biological and Chemical Applications. *J. Phys. Chem.* **1993**, *97* (6), 1101–1109.
- (32) Rashin, A. A. Buried Surface-Area, Conformational Entropy, and Protein Stability. *Biopolymers* **1984**, *23* (8), 1605–1620.
- (33) Chong, L. T.; Duan, Y.; Wang, L.; Massova, I.; Kollman, P. A. Molecular dynamics and free-energy calculations applied to affinity maturation in antibody 4G8G7. *Proc. Natl. Acad. Sci. U. S. A.* **1999**, *96* (25), 14330–14335.
- (34) Reyes, C. M.; Kollman, P. A. Structure and thermodynamics of RNA-protein binding: using molecular dynamics and free energy analyses to calculate the free energies of binding and conformational change. *J. Mol. Biol.* **2000**, *297* (5), 1145–1158.
- (35) Wang, J.; Morin, P.; Wang, W.; Kollman, P. A. Use of MM-PBSA in reproducing the binding free energies to HIV-1 RT of TIBO derivatives and predicting the binding mode to HIV-1 RT of efavirenz by docking and MM-PBSA. *J. Am. Chem. Soc.* **2001**, *123* (22), 5221–5230.
- (36) Cheatham, T. E., 3rd; Srinivasan, J.; Case, D. A.; Kollman, P. A. Molecular dynamics and continuum solvent studies of the stability of polyG-polyC and polyA-polyT DNA duplexes in solution. *J. Biomol. Struct. Dyn.* **1998**, *16* (2), 265–280.
- (37) Bashan, A.; Agmon, I.; Zarivach, R.; Schluenzen, F.; Harms, J.; Berisio, R.; Bartels, H.; Franceschi, F.; Auerbach, T.; Hansen, H. A.; Kossoy, E.; Kessler, M.; Yonath, A. Structural basis of the ribosomal machinery for peptide bond formation, translocation, and nascent chain progression. *Mol. Cell* **2003**, *11* (1), 91–102.
- (38) Champney, W. S. Bacterial ribosomal subunit assembly is an antibiotic target. *Curr. Top. Med. Chem.* **2003**, *3* (9), 929–947.
- (39) Omura, S. *Macrolide Antibiotics: Chemistry, Biology, and Practice*, 2nd ed.; Academic Press: Amsterdam, Boston, 2002; p 637.
- (40) Bertho, G.; Gharbi-Benarous, J.; Delaforge, M.; Girault, J. P. Transferred nuclear Overhauser effect study of macrolide-ribosome interactions: correlation between antibiotic activities and bound conformations. *Bioorg. Med. Chem.* **1998**, *6* (2), 209–221.
- (41) Otyepka, M.; Kriz, Z.; Koca, J. Dynamics and binding modes of free cdk2 and its two complexes with inhibitors studied by computer simulations. *J. Biomol. Struct. Dyn.* **2002**, *20* (2), 141–154.
- (42) Pricl, S.; Fermeglia, M.; Ferrone, M.; Tamborini, E. T315I-mutated Bcr-Abl in chronic myeloid leukemia and imatinib: insights from a computational study. *Mol. Cancer Ther.* **2005**, *4* (8), 1167–1174.
- (43) Adekoya, O. A.; Willassen, N. P.; Sylte, I. Molecular insight into pseudolysin inhibition using the MM-PBSA and LIE methods. *J. Struct. Biol.* **2006**, *153* (2), 129–144.
- (44) Xu, Y.; Wang, R. A computational analysis of the binding affinities of FKBP12 inhibitors using the MM-PB/SA method. *Proteins* **2006**, *64* (4), 1058–1068.
- (45) Liu, B.; Bernard, B.; Wu, J. H. Impact of EGFR point mutations on the sensitivity to gefitinib: insights from comparative structural analyses and molecular dynamics simulations. *Proteins* **2006**, *65* (2), 331–346.

- (46) Gouda, H.; Kuntz, I. D.; Case, D. A.; Kollman, P. A. Free energy calculations for theophylline binding to an RNA aptamer: Comparison of MM-PBSA and thermodynamic integration methods. *Biopolymers* **2003**, *68* (1), 16–34.
- (47) Page, C. S.; Bates, P. A. Can MM-PBSA calculations predict the specificities of protein kinase inhibitors. *J. Comput. Chem.* **2006**, *27* (16), 1990–2007.
- (48) Kuhn, B.; Gerber, P.; Schulz-Gasch, T.; Stahl, M. Validation and use of the MM-PBSA approach for drug discovery. *J. Med. Chem.* **2005**, *48* (12), 4040–4048.
- (49) Bren, M.; Florian, J.; Mavri, J.; Bren, U. Do all pieces make a whole? Thiele cumulants and the free energy decomposition. *Theor. Chem. Acc.* **2007**, *117* (4), 535–540.
- (50) Bren, U.; Martinek, V.; Florian, J. Decomposition of the solvation free energies of deoxyribonucleoside triphosphates using the free energy perturbation method. *J. Phys. Chem. B* **2006**, *110* (25), 12782–12788.
- (51) Yonath, A. Antibiotics targeting ribosomes: resistance, selectivity, synergism, and cellular regulation. *Annu. Rev. Biochem.* **2005**, *74*, 649–679.
- (52) Moazed, D.; Noller, H. F. Chloramphenicol, erythromycin, carbomycin and vernamycin B protect overlapping sites in the peptidyl transferase region of 23S ribosomal RNA. *Biochimie* **1987**, *69* (8), 879–884.
- (53) Tenson, T.; Mankin, A. S. Short peptides conferring resistance to macrolide antibiotics. *Peptides* **2001**, *22* (10), 1661–1668.
- (54) Tu, D.; Blaha, G.; Moore, P. B.; Steitz, T. A. Structures of MLSBK antibiotics bound to mutated large ribosomal subunits provide a structural explanation for resistance. *Cell* **2005**, *121* (2), 257–270.
- (55) Pfister, P.; Jenni, S.; Poehlsgaard, J.; Thomas, A.; Douthwaite, S.; Ban, N.; Bottger, E. C. The structural basis of macrolide-ribosome binding assessed using mutagenesis of 23S rRNA positions 2058 and 2059. *J. Mol. Biol.* **2004**, *342* (5), 1569–1581.
- (56) Leclercq, R.; Courvalin, P. Resistance to macrolides and related antibiotics in *Streptococcus pneumoniae*. *Antimicrob. Agents Chemother.* **2002**, *46* (9), 2727–2734.
- (57) Schlunzen, F.; Harms, J. M.; Franceschi, F.; Hansen, H. A. S.; Bartels, H.; Zarivach, R.; Yonath, A. Structural basis for the antibiotic activity of ketolides and azalides. *Structure* **2003**, *11* (3), 329–338.
- (58) Wodak, S. J.; Belle, D. v.; Prevost, M. Molecular dynamics and free energy calculations applied to the enzyme barnase and one of its stability mutants. In *Computer Modelling in Molecular Biology*; Goodfellow, J. M., Ed.; VCH: Weinheim, New York, 1995; pp 62–102.
- (59) Humphrey, W.; Dalke, A.; Schulten, K. VMD: visual molecular dynamics. *J. Mol. Graph.* **1996**, *14* (1), 27–38.

CI8003495